LIDIJA D. RAFAILOVIĆ[1]
DRAGICA M. MINIĆ[2]

[1]Physics of Nanostructured Materials, Faculty of Physics,University of Vienna, Austria
[2]Faculty of Physical Chemistry, University of Belgrade, Serbia

REVIEW PAPER

UDC 544.6:669.24'25:66

DOI: 10.2298/HEMIND0905557R

DEPOSITION AND CHARACTERISATION OF NANOSTRUCTURED NICKEL-COBALT ALLOYS*

Nanostructured nickel and cobalt alloy disperse deposits were obtained galvanostatically on Cu substrates from ammonium sulfate chloride electrolytes. The influence of current density and the Ni^{2+}/Co^{2+} ratio in the bath on the microstructure and phase composition of the Ni–Co deposits were studied. It was shown that both bath composition and current density influence strongly the deposit growth mechanism as well as the deposit composition, microstructure, grain size and surface morphology. When electrodeposition was performed at high overpotentials, far from equilibrium conditions, face-centered cubic (FCC) mixtures of Ni and Co were generated while at low overpotentials, as well as at higher content of cobalt in the electrolyte, hexagonal close packed (HCP) Co was formed with a lower rate of hydrogen evolution. The increase in the concentration of HCP phase in the nanocrystalline deposits was caused by increasing the overall Co content in the materials prepared as well as by decreasing deposition current density. The effects of structural changes on magnetic properties of the electrochemically obtained nanocrystalline deposits were studied in the temperature interval from room temperature to 600 °C. It was shown that each stage of the structural changes caused corresponding changes in the magnetic permeability for the alloys prepared.

From the earliest papers in the nanostructured material science [1] until nowadays and from widespread research over the past couple of decades, nanoscaled materials have attracted a lot of attention of scientists all over the world concerning both scientific as well as technological aspect [2–4]. Nanostructured materials provide an excellent opportunity to extend the understanding of the structure–property relations in solid materials and also open an attractive potential for technological applications [5–9].

Many synthesis techniques for production of nanostructured materials have been developed like inert gas--condensation, ball-milling, severe plastic deformation, chemical vapor deposition and electrochemical deposition [3]. Although electrodeposition has been one of the methods using well-known processes for synthesizing nanocrystalline materials, properties of nanocrystalline electrodeposits are less evaluated, especially for tribological application in nanoscale devices such as micro- and nano-electromechanical systems (MEMS and NEMS). The electrodeposition technique has significant advantages compared to other methods for synthesis of nanocrystalline materials; one of them is possibility of preparation of amorphous alloys [8]. Other important advantages are the easy preparation of materials of high purity exhibiting different structures and morphologies and the possibility of changing the composition and morphology within a broad range, adjusting only the deposition parameters [10–12].

Corresponding author: D. Minić, Faculty of Physical Chemistry, University of Belgrade, Studentski trg 12–16, 11000 Belgrade, Serbia.
E-mail: dminic@ffh.bg.ac.rs
Paper received: 1 October, 2009.
Paper accepted: 12 October, 2009.
*Invited paper on the occasion of the 20th anniversary of the Society of Physical Chemists of Serbia, 2009.

Electrodeposited Ni–Co thin films have been intensively studied due to their application in MEMS [6]. Thin and thick Ni–Co films form important parts of magnetic-MEMS devices including sensors, microactuators or micromotors because of their excellent physical properties. Fine Ni, Co and Ni–Co alloy powders are required for developing magnetoresistive sensors in thick-film form [7].

Electrodeposition of Ni–Co powders from defined solutions of Ni powders as well as of Co powders were established by the work of Calusaru [8]. Almost all metals can be obtained in powder form, but the method for obtaining such materials will be dependent on intended properties affected by their structure [10]. The electrolytic powder production method usually yields a product of requested chemical composition, high purity, which can be well pressed and sintered as we have show in previous papers [11–13].

The electrodeposition of Co has been far less studied compared to the Ni electrodeposition [14]. Electrolytic Co crystallizes with two modifications, the HCP, stable allotropic modification at temperatures below 417 °C, and with the FCC form of lattice structure stable at higher temperatures. With increase of pH the structure becomes completely in the form of the HCP-phase and deposit texture depends mainly on solution pH [15]. The prevailing orientations and their stability with respect to the operative conditions are characterized in details for both sulphate [15] and chloride-based electrolytes [16]. Cohen-Hyams *et al*. showed that the structure of electrodeposited Co significantly depends on the level of used overpotential [17]. When electrodeposition is performed far from equilibrium conditions, *i.e*. at a higher overpotentials, FCC cobalt is deposited while at lower overpotentials HCP Co is formed with a lower rate of hydrogen evolution.

Recently, several papers have been published on the effect of electrolyte composition and current density on the hardness of the electrodeposited iron group films [18] as well as on the chemical composition, structure, electric and magnetic properties and corrosive stability of thin electrodeposited nanocrystalline film [19–29]. Higher electrical resistivity of the electrodeposited Ni–Co alloys can be attributed to the smaller grain sizes, high defect densities, and impurity incorporation during electrodeposition [5].

Alloys of iron group metals, Fe, Co and Ni, have been considered as very good magnetic materials [19,20]. These alloys are known to possess much better permanent magnetic properties than pure metals.

In the present paper the composition, the morphology and microstructure of Ni–Co non-compact deposits galvanostatically deposited were investigated as well as their thermal stability and structural transformations in the temperature range from ambient to 650 °C[11–13,27–36].

EXPERIMENTAL PROCEDURES

A differently composed Ni–Co alloys were prepared galvanostatically from ammonium sulfate chloride solutions, containing different Ni^{2+}/Co^{2+} concentration ratios of 4, 1 and 0.25 (total concentrations: 0.12 mol dm^{-3} ($NiSO_4$+$CoSO_4$), 0.5 mol dm^{-3} NH_4Cl and 3.5 mol dm^{-3} NH_4OH) at pH 10 in a glass cell with a volume of 1.0 dm^3 without stirring, thermostatically controlled at a temperature of 298±1 K. Cu platelets placed in the center of the cell with a 1.0 cm^2 surface area and 0.2 cm thickness were used as working electrodes. Ti plate covered with RuO_2/TiO_2 (10 cm^2 geometric area), placed close and parallel to the Cu plate, was used as anode (DSA). The electrodeposition of the powder was performed with a constant current regime in the range of 40−450 mA cm^{-2} [27–29].

Polarization measurements were performed using a computer controlled electrochemical system (PAR M 273A, software PAR M352/252, version 2.01) with a sweep rate of 1 mV s^{-1}. For the correction of the IR drop, current interrupt technique was used with a time of current interruption of 0.5 s. The counter electrode (Pt-foil) and the reference electrode (saturated calomel electrode, SCE) were placed in separate compartments. The Luggin capillary connecting the SCE to the electrolyte was positioned at a distance of 0.2 cm from the working electrode (copper rod, d = 0.4 cm). Before each experiment, the working electrode was polished using a 0.05 μm alumina impregnated polishing cloth.

The current efficiency was determined at different current densities by measuring the hydrogen evolution on the working electrode. Working electrode was placed in the middle of the cell under the burette with the surface facing up so that the whole amount of the evolved hydrogen goes into the burette [13]. Burette was also kept at the same temperature. After each experiment with constant current, electrode was taken from the solution, remained deposit was removed and its surface was again polished by the same procedure. At each applied current density, hydrogen was collected starting from a clean electrode surface, as it was in the case for measuring the polarization curves.

The current for hydrogen evolution was obtained using equation for Faraday's low applied to the process of gas evolution:

$$j_{H_2} = \frac{nFV_0}{tV_n}$$

where V_0 is the experimentally determined volume of the hydrogen at p (atm) and T = 298 K, t − the time of hydrogen evolution under constant current, V_n − the volume of the 1 mol of hydrogen at normal condition (22.4 dm^3 mol^{-1}), n − the number of exchanged electrons and F is the Faraday's constant.

Current efficiency for the electrodeposition process was obtained from the relation:

$$\eta = \frac{j_{tot} - j_{H_2}}{j_{tot}} \times 100$$

Alternatively, current efficiency was determined directly by measuring the mass of electrodeposited Ni–Co alloy on the cathode at different current densities [26]. The mass of the cathode was measured on analytical balance (Kern 770) before and after the electrodeposition process on the constant current at time. These results were compared with the theoretical one obtained from the equation for Faraday's low. The current efficiency was determined on the base of difference of the mass theoretically expected and experimentally obtained.

For the surface morphology characterisation an XL 30 ESEM-FEG (environmental scanning electron microscope with field emission gun, FEI Company, Netherlands) was used. The 3D reconstruction of the specimen surface shown was characterized by scanning electron microscope (SEM) using MeX software from Alicona (A).

An alloy composition analysis was performed by ESEM using EDX software Genesis, USA. X-ray powder diffraction (XRD) analysis was carried out using a MRD diffractometer (Philips, NL) with CuKα radiation (40kV/30 mA). Step-scan mode was utilized with 0.03° in 2θ per 1.15 s step. The angular 2θ range investigated was 30–110°. Structural transformations of the alloy deposits were determined upon annealing the samples at selected temperatures for 30 min in an argon atmosphere.

DSC measurements were performed at 10 mg samples using a DSC-204 C (Netzsch, D) in the temperature range of 25 to 600 °C in argon atmosphere with a heating rate of 20 K min^{-1}. For magnetic measurements,

the non-compact deposits were pressed at 100 MPa into 40 mm long, 1 mm wide and 0.3–0.6 mm thick samples. The determination of the relative magnetic permeability was performed using a modified Maxwell method, based on the action of an inhomogeneous magnetic field on the sample, using home-made equipment [13].

RESULTS AND DISCUSSION

Figure 1 shows the polarization curves of the Cu cathode for different compositions of the electrolyte. The shape and position of the polarization curves strongly depend on the electrolyte composition. Decreasing the amount of Co^{2+} and increasing the amount of Ni^{2+} shift the position of corresponding polarization curves towards negative values of potentials, corresponding to the potential of the Ni/Ni^{2+} deposition of pure nickel. According to this polarization curves, current densities of 40–400 mA cm^{-2} were selected for deposition of the alloys, expecting the formation of non--compact deposits [40].

A defined amount of Ni–Co alloy was possible to obtain only at current density, j > 40 mA cm^{-2}. However, in all bath compositions at current densities, j < 65 mA cm^{-2}, compact deposits were obtained. For higher current densities (> 150 mA cm^{-2}), the deposits were in the form of powders that could be easily removed from the electrode surface. It should be mentioned that for higher current densities, hydrogen evolution was quite intensive providing conditions in which some amount of the powders drop into the cell. The trend for the hydrogen evolution reaction which is accomplished with alloy powder deposition reaction at the current density, j >150 mA cm^{-2} increases with a decrease of the amount of Ni^{2+} in the electrolyte suggesting that activity for the hydrogen evolution reaction increases with a decrease of the nickel content in the deposit.

The hydrogen evolution during deposition of the alloys affects the current efficiency, depending on the electrolyte composition as well as on the current density (Figure 2). In the current density range where disperse deposits were deposited, the current efficiency decreases with the increasing the current density and with the decrease of the Ni^{2+} concentration in the electrolyte.

Chemical composition of deposits

The compositions of the alloys galvanostatically deposited, calculated for alloy samples of surfaces of 10 μm^2 with an error of ±2%, are summarized in Table 1.

According to the EDX results, the increase in current density leads to an increase of the Ni content in the deposits. At current density of j = 65 mA cm^{-2}, the content of cobalt in the alloys is always higher than in the electrolyte, as a consequence of the lower overpotential for the Co^{2+} reduction compared to Ni^{2+} as can be seen also from the polarization curves (Figure 1b).

The deposits (alloys 3, 4 and 5) obtained out of a 1:1 electrolyte using selected current densities, exhibit different compositions as well as structures. Increasing the current density shifts the ratio of nickel and cobalt in the alloys closer to the value of concentration of the corresponding ions in electrolyte. The phenomenon of anomalous co-deposition (characteristic for the electrodeposition of iron group metals) is very pronounced in the production of compact deposits. However, in the case of non-compact/disperse deposits, anomalous co-deposition is much less pronounced, so that the composition of the alloy powder deposited at high current

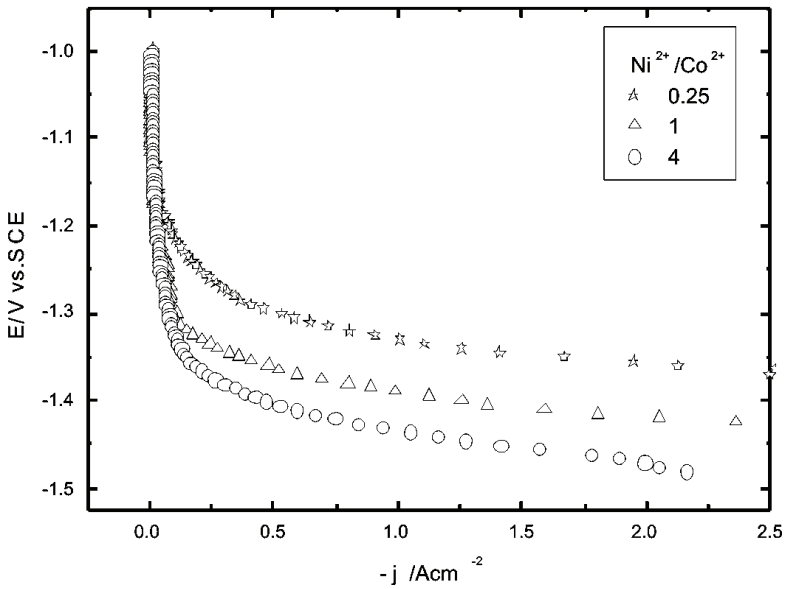

Figure 1. Polarization curves at the Cu cathode for the different compositions of the electrolyte: a) Ni^{2+}/Co^{2+} = 4; b) Ni^{2+}/Co^{2+} = 1 and c) Ni^{2+}/Co^{2+}=0.25, sweep rate: 1mV s^{-1}.

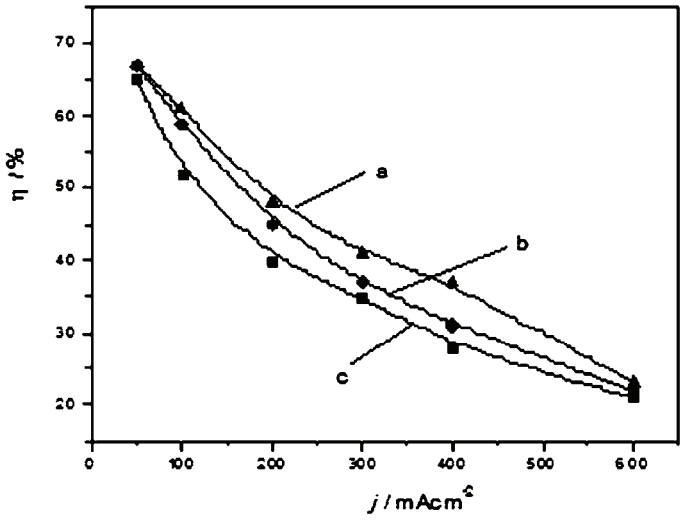

Figure 2. Current efficiency of the alloy deposition process at a Cu cathode vs. the current density for different composition of electrolyte: a) Ni^{2+}/Co^{2+} = 4; b) Ni^{2+}/Co^{2+} = = 1 and c) Ni^{2+}/Co^{2+} =0.25.

density is almost similar to the concentration of the metal ions in the electrolyte (alloy 5).

Morphology of nanostructured deposits obtained from bath of different compositions

Figure 3 presents SEM micrographs (micrographs a–c) of the alloys, electrodeposited from electrolytes with three different Ni^{2+}/Co^{2+} concentration ratios (4, 1, 0.25, respectively) at a current density of j = 65 mA cm^{-2}, as well as the corresponding 3D SEM micrographs (Figure 4, micrographs a–c). For current densities in the range between 65 and 400 mA cm^{-2}, deposits were obtained with the size of agglomerates varying from 5 μm to about 50 μm.

The deposit with the highest content of Ni^{2+} in the electrolyte (micrographs 3a and 4a) exhibits the cauli-

Table 1. Chemical composition of the alloys (at%) galvanostatically deposited from electrolytes with the different ratios of Ni^{2+}/Co^{2+} and at the different current densities

Metal	Ni^{2+}/Co^{2+}				
	4:1 (Alloy 1)	1:4 (Alloy 2)	1:1 (Alloy 3)	1:1 (Alloy 4)	1:1 (Alloy 5)
	j / mA cm^{-2}				
	65	65	65	220	400
Ni	80	5.5	33	40	43
Co	20	94.5	67	60	57

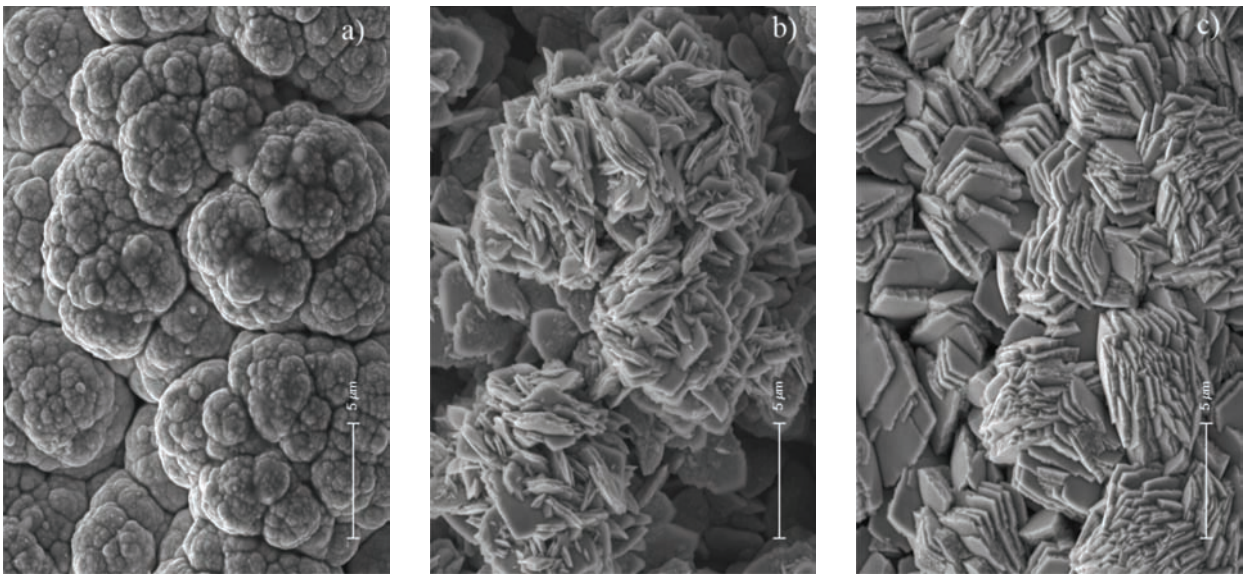

Figure 3. SEM micrographs of Ni–Co deposits obtained in the galvanostatic regime at a current density of 65 mA cm^{-2}. The concentration ratio Ni^{2+}/Co^{2+} in the electrolyte was: 4:1 (a), 1:1 (b) and 1:4 (c).

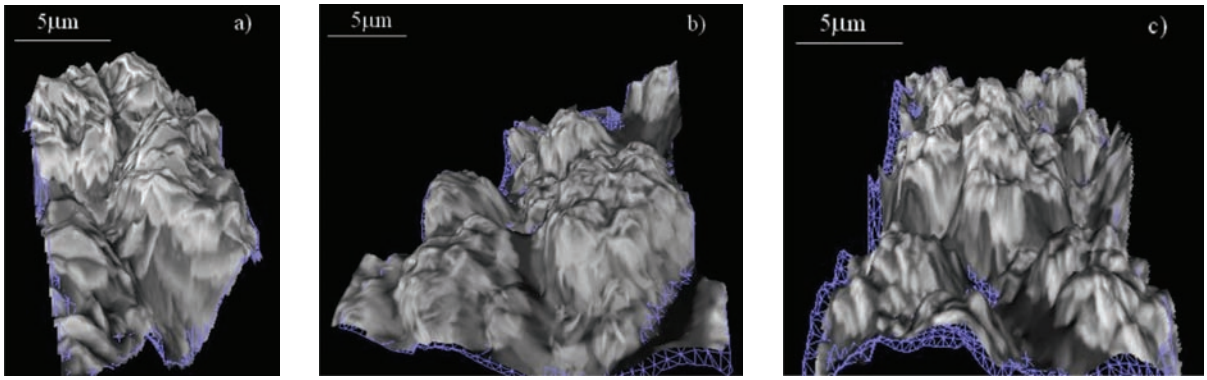

Figure 4. 3D SEM reconstructions of the surfaces of Ni−Co deposits from an electrolyte with concentration ratio Ni^{2+}:Co^{2+} =1:1 at different current densities: a) 65, b) 220 and c) 400 mA cm^{-2}. (Figure 4a corresponds to Figure 3b).

flower-like structure, consisting of small particles with an average radii < 500 nm, surrounded with diffusion zones and the deposition took place in spherically symmetrical way. For the ratio of Ni^{2+}/Co^{2+} = 1 (micrographs 3b and 4b), the morphology of the deposit is changed and the powder consists of particles also with cauliflower structure but exhibiting a different surface morphology, based on preferred oriented platelets (Figure 3b). Finally, the particles deposited from electrolyte with the highest content of Co^{2+} (micrographs 3b and 4c) show the platelet structure, also with preferred orientation and a size of the platelets in the μm range. Concluding, the morphology of electrodeposited alloy depends strongly of the electrolyte composition. The surface morphology of the deposits is determined by the nature of the electrochemically active ions or complexes and kinetics of the electrocrystallization processes. Overpotentials of 1.3 V are needed for the deposition of very disperse deposit [39].

The 3D dataset was calculated from two stereoscopic images obtained by tilting the sample stage in the ESEM at the eucentric point with an angle of 5°. It enables to carry out a 3D analysis directly from the digital images yielding profile and roughness measurements and also area analysis as well as volumetric measurements. The calculated roughness parameters are shown in Table 2 (*Ra* − mean roughness, *Rz* − the difference between the highest and the lowest point in the picture of defined scan, *RS* − active surface, the ratio of the real surface including topography to a projected surface of the measurements (a square with dimensions of (23×15) μm)).

A concentration ratio Ni^{2+}/Co^{2+} of 4 and 1 led to a surface with similar roughness values in spite of different morphology, Figures 3a and 3c, respectively. In the case of concentration ratio Ni^{2+}/Co^{2+} = 1, the mean roughness of the deposit is almost 3 times higher than in the specimens with ratios of 4 or 0.25. Also, the active surface has a maximum at the ratio 1. An increase in the current density results in a decrease in roughness, since at higher current densities the amount of crystal nuclei on the surface in enhanced and dendritic growing is reduced in the initial period of deposition.

Microstructure of the nanostructured Ni−Co deposits

The crystal structure, particle shape and size of the electrochemically obtained cobalt–nickel alloy deposits considerably depend on current density according to the ESEM analysis and X-ray diffraction patterns (Figure 5). Average grain sizes and lattice parameters were calculated from the peak broadening using Scherrer equation with Rietveld refinement method [40]. Powder particles obtained with the geometric size varying from 5 μm to about 50 μm were composed by fine nanosized crystallites (see Table 3). Crystal structure and composition of the deposits obey the phase diagram [41].

SEM micrographs of alloy deposited from electrolyte with concentration ratio Ni^{2+}/Co^{2+} = 1 at different current densities, j = 65 mA cm^{-2} (Figure 4a), j = = 220 mA cm^{-2} (Figure 4b) and j = 400 mA cm^{-2} (Figure 4c), show significant differences in the morphology as well as in the particle size. The increase of current density from j = 65 mA cm^{-2} to j = 220 mA cm^{-2} changes the

Table 2. Roughness parameters of alloys deposited from electrolytes of different Ni^{2+}/Co^{2+} concentration ratio and at different current densities

Alloy	Current density, mA cm^{-2}	*Ra* / μm	*Rz* / μm	*RS*
1	65	1.0	4.7	1.64
2	65	0.7	4.7	1.64
3	65	3.0	13.1	1.98
4	220	1.1	5.2	1.38
5	400	1.0	6.5	1.62

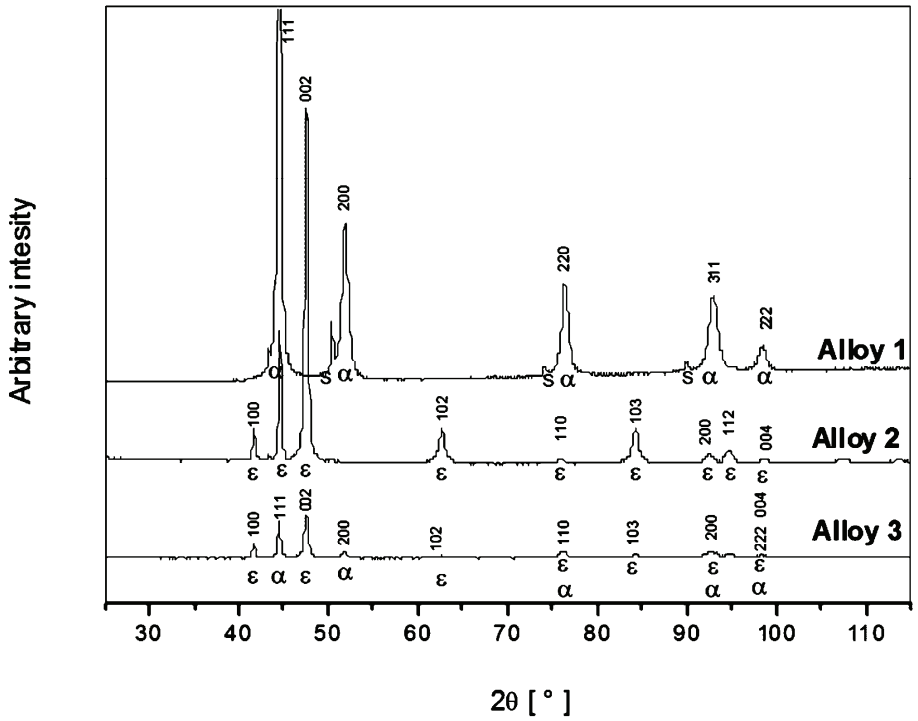

Figure 5. X-ray diffraction patterns of alloys 1, 2 and 3 (α – reflections attributed to the α-Ni; ε – reflections attributed to the ε-Co; S – reflection attributed to the Cu substrate).

morphology of deposit from the inlaid structure to the cauliflower-like structure with a finer grain size. Further increasing of current density shows no significant influence on particle size.

Figure 5 presents X-ray diffraction patterns of three alloys, electrodeposited at a current density of j =65 mA cm^{-2}, with 43 mAh cm^{-2} consumed and average sample thickness of 25±5 μm. The phase composition and average size of crystallites for all five prepared alloys are summarized in Table 3.

As can be seen from the presented results (Figure 5 and Table 3), a deposit obtained from the electrolyte with Ni^{2+}/Co^{2+} concentration ratio 4:1 (alloy 1) consists of α-Ni phase with face-centered cubic lattice (FCC phase, space group Fm3m, a = 3.524Å, JCPDS 00-004--0850). The diffraction peaks of Cu with low intensity result from the substrate material. The average size of primary crystallites in the FCC phase was 13±2 nm. The alloy electrodeposited at the same current density with the ratio Ni^{2+}/Co^{2+} = 0.25 (alloy 2) contains the ε-Co phase with hexagonal close-packed lattice (HCP phase, space group P63/mmc, a = 2.506Å, c = 4.069Å, JCPDS card 01-071-4239). With increasing Co content in the alloys (Table 3) the average size of crystallite increases ranging from 13 to 19 nm for the FCC phase and from 15 to 20 nm for the HCP phase. The diffraction patterns of all three alloys deposited at relatively low current density show a strong texture.

A detailed Rietveld analysis revealed that Ni–Co alloys deposited from the electrolyte with the Ni^{2+}/Co^{2+} ratio of 1 at different current densities (alloys 3–5), are composed of solid solutions of the both, cubic FCC

Table 3. Phase composition, size of primary crystallites and cell parameters of the alloys electrodeposited

Alloy	Crystal structure/Content (%)	Grain size, nm	a / Å	c / Å	Cell volume, Å^3
1	FCC/100	13	3.526	–	43.833
2	HCP/100	20	2.506	4.069	22.126
3	FCC/28	19	3.529	–	43.955
	HCP/72	15	2.505	4.072	22.127
4	FCC/71	13	3.529	–	43.971
	HCP/27	11	2.499	4.077	22.043
	amorphous phase/8	–	–	–	–
5	FCC/82	11	3.533	–	44.096
	HCP/3	10	2.495	4.100	22.100
	amorphous phase/15	–	–	–	–

phase and the HCP phase due to the mutual miscibility of Ni and Co in the range of concentration in the obtained deposits (Figure 6 and Table 3). The increase of current density lead to the increase in the content of FCC phase in solid solution as well as the formation of significant amounts of amorphous phase.

An analysis of the diffractograms of the powdered alloys electrodeposited at 65 and 400 mA cm^{-2} (alloys 3–5) shows that the decrease of the current density results in pronounced crystallization and an increase of the size of crystallites as well as higher HCP content. Furthermore, it can be seen that the cell volume of the alloys (alloys 3–5) increases slightly with increasing current density. Alloy 1 (rich in Ni) and alloy 2 (rich in Co) exhibit cell volumes comparable to the theoretical values of Ni (43.8 $Å^3$) and Co (22.1 $Å^3$).

At lower current densities, the content of Co in the deposit consists only of HCP phase; with increasing current density the content of Co decreases by approximately 10 at%, but the concentration of the HCP phase is reduced down to 3%. Beside an amorphous content of 8–15%, the rest of the Co is forming a solid solution within the Ni FCC phase, resulting in an increase of the cell volume (see Table 3). If the kinetics of the deposition process is fast, the deposit can be obtained at low driving force [29], while a much larger driving force is needed for kinetically slow processes such as Ni and Co deposition, resulting in an electrodeposition process far from equilibrium conditions, *i.e.* at high overpotentials, and formation of the FCC phase. At low overpotentials, a higher amount of Co as the HCP phase is formed.

Thermal stability of nanostructured deposits

The thermal stability of alloys (prepared as non-compact deposits from the electrolytes with concentration ratios in the bath Ni^{2+}/Co^{2+} = 4, alloy 1, and Ni^{2+}/Co^{2+} = 0.25, alloy 2, at j = 65mA cm^{-2} was characterized by DSC analysis (temperature range from room temperature to 600 °C) as well as by X-ray diffraction and SEM. For X-ray diffraction and SEM measurements, the samples were annealed in sealed evacuated quartz tubes at selected temperatures for 30 min, water quenched and then analyzed.

Since at the nanometer scale the atomic fraction of interfacial atoms is comparable to that in the perfect crystalline state, the structure of grain joints is unstable at room temperature and tends to evolve towards a more ordered state. Because the intercrystalline volume represents a region of stored excess energy with respect to the bulk of a grain, there is a significant driving force for grain growth in nanocrystalline materials during heating. The structure of nanosized metals is thus thermodynamically unstable and shows a strong tendency to structural changes under annealing [42] or even at room temperature [43]. These changes typically affect the density of crystalline defects, grain size, crystallographic orientation and grain boundary structure [44]. The enthalpy release due to annealing of the nanocrystalline structure can be directly measured, *e.g.* by DSC [45].

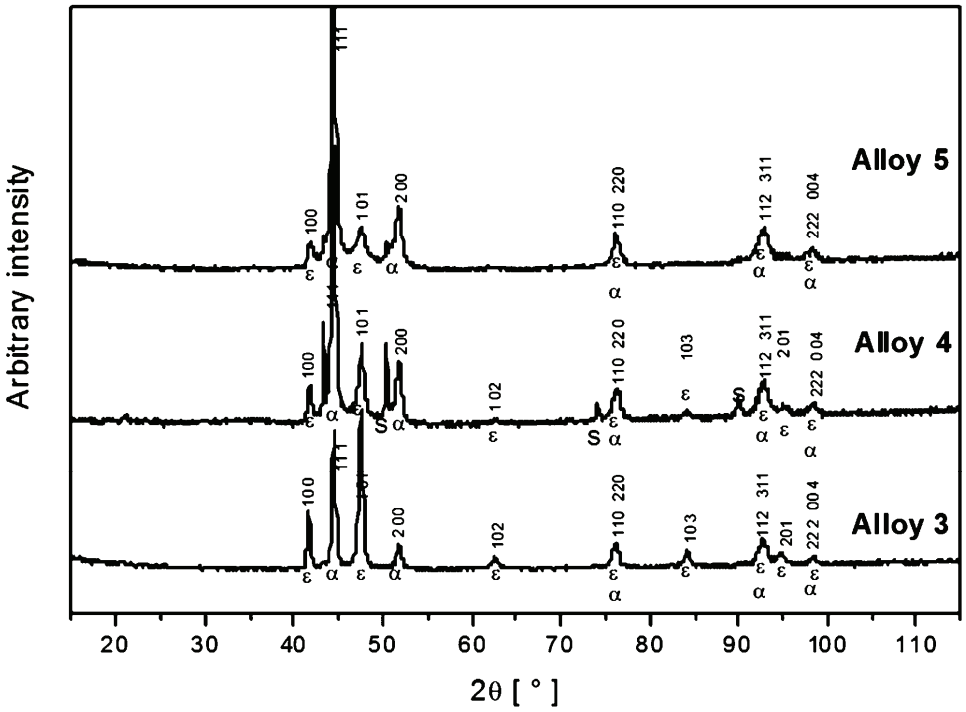

Figure 6. X-ray diffraction patterns of the alloys 3–5 (α – reflections attributed to the α-Ni; ε– reflections attributed to the ε-Co; S – reflection attributed to the Cu substrate).

The thermal behavior of the non-compact alloy 1 is depicted in DSC curves, Figure 7. The heat release associated with structural relaxation in the temperature range 120–300 °C was ΔH = –10.3 J/g and for further structural transformations in the temperature range 380––530 °C, released heat was ΔH = –25.8 J/g.

Structural transformations in Ni–Co deposits (alloy 1) induced by annealing at 250, 350 and 550 °C are confirmed by XRD (Figure 8). These temperatures have been chose according to DSC curve. The XRD patterns and Rietveld refinement analysis (Table 4) show only grain growth. No reflections related to cobalt or nickel oxides were detectable. A typical SEM micrograph of alloy 1 after annealing at 550 °C is shown in Figure 9. The composition as well as the structure of the deposit was attained with no significant change even in particle size.

As in many studies on the thermal stability of nanocrystalline materials [46], the Ni–Co disperse alloy exhibits a quasi-nucleation growth-process. When nanocrystalline deposits are brought to an elevated temperature, the nanometer-sized crystallites in the deposits start to grow in a random, non-uniform way and some of the present nanocrystallites appear as nuclei and preferentially start to grow at the expense of the surrounding nanocrystalline matrix. With increasing temperature,

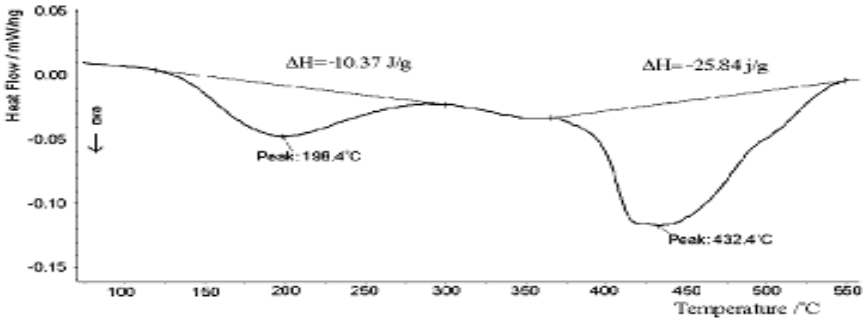

Figure 7. DSC of the alloy 1; heating rate 20 K min^{-1}.

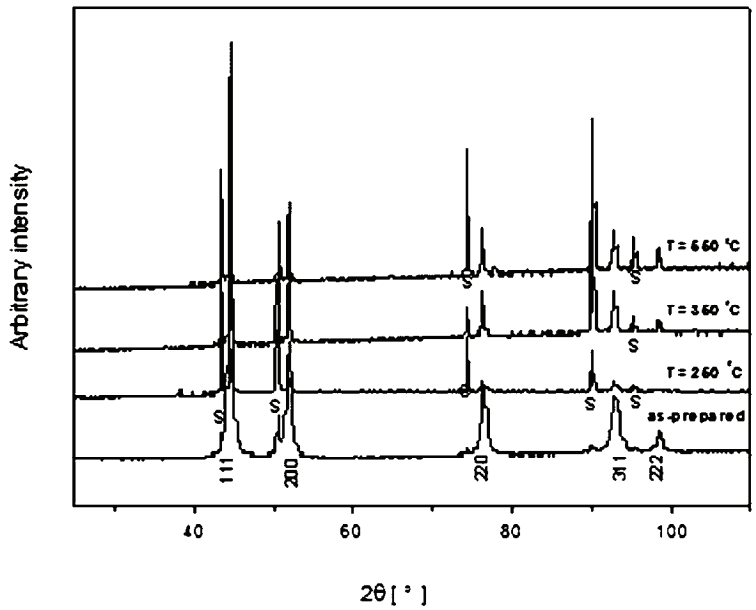

Figure 8. XRD patterns of alloy 1 as prepared and annealed at different temperatures.

Table 4. Phase composition and size of crystallites of electrodeposited as well as annealed alloy 1

Treatment	Crystal structure	Grain size, nm	Lattice constant, Å	Cell volume, Å^3
As prepared	FCC	13	3.526	43.833
Annealed at 250°C	FCC	20	3.527	43.891
Annealed at 350°C	FCC	47	3.527	43.876
Annealed at 550 °C	FCC	57	3.530	44.004

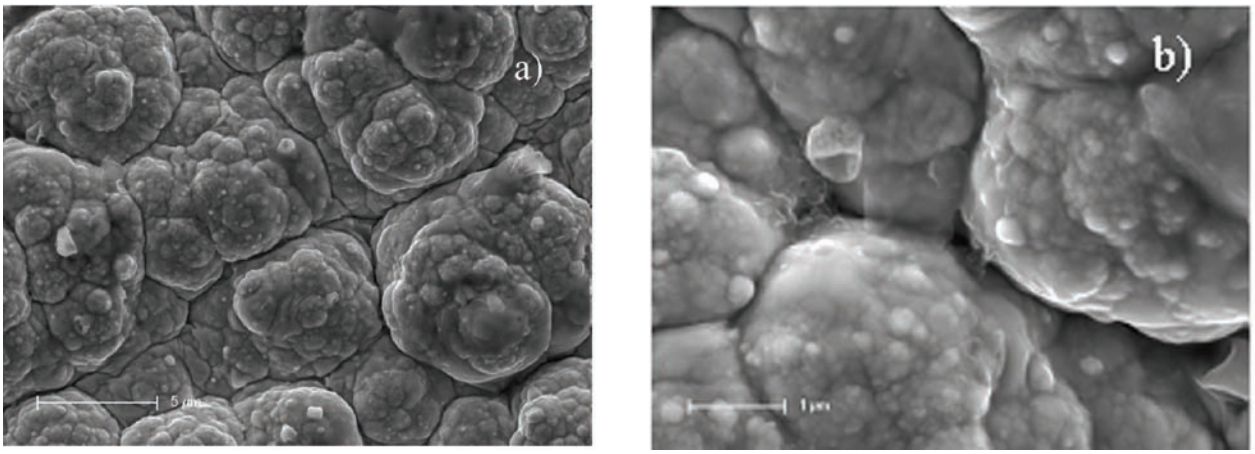

Figure 9. SEM micrographs of Ni–Co deposits on copper substrate prepared out of an electrolyte with concentration ratio Ni^{2+}/Co^{2+} = = 4, j = 65 mA cm^{-2}, upon annealing at 550 °C; a) magnification 5000×; b) magnification 20000× (SE, accelerating voltage: 10 kV).

the grains become larger and the number of dislocations decreases considerably. The lattice constant of the FCC phase increases slightly with increased annealing temperature, resulting in large cell volumes compared to the theoretical face centered cubic (FCC) nickel, probably due to the presence of 20 percentage of cobalt in the deposit (Table 4).

The thermal behavior of the of Ni–Co alloy 2 (electrolyte ratio Ni^{2+}/Co^{2+} = 0.25, j = 65 mA cm^{-2}) shown on the DSC curve, Figure 10, is characterized by an exothermic reaction indicating a stepwise process of structural relaxation and transformation of the alloy in the temperature range 300–550 °C. The first exothermic feature in the temperature range 280–300 °C can be attributed to structural relaxation process of the FCC phase. During grain growth, as the system moves from the condition of an as-prepared nanocrystalline sample of higher excess free energy to the condition of the annealed sample exhibiting lower excess of free energy, there is an enthalpy release of ΔH = –190.6 J/g) giving a measure of the thermal stability of the sample connected with the phase transformation from HCP to FCC structure.

The XRD of the alloy 2 as prepared on the copper substrate showed only the reflections of a Co-like HCP pattern, see Figure 5. According to the X-ray diffraction analysis (Figure 11), during annealing the concentration of the HCP phase is continuously reduced and the reflection attributed to the FCC phase of Co appears, with a content of > 70% in the sample, Table 5.

The grain size of the FCC phase significantly increases to 50 nm, while size of HCP phase decreases to 6.5 nm (Table 5). Annealing at temperatures of 280 and 350 °C caused only slight difference of grain size and lattice constant (Table 5). However, the annealing at temperature of 550 °C generated grain size and lattice constant changes due to the austenitic allotropic phase transformation at 422 °C according to the phase diagram [43]. The HCP phase is more stable phase at room temperature, but reverse transformation to FCC phase after

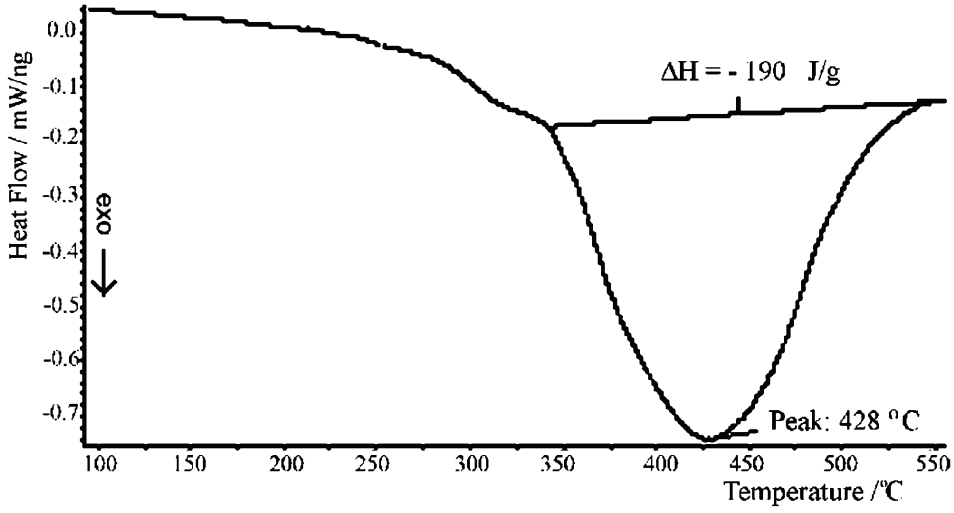

Figure 10. DSC of the alloy 2; heating rate: 20 K min^{-1}.

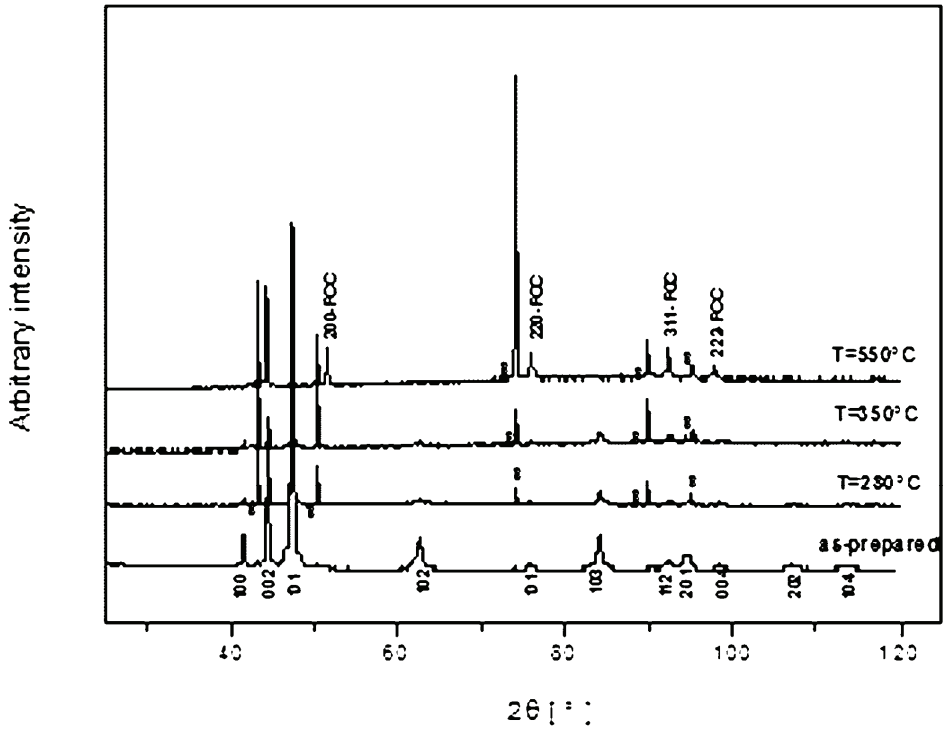

Figure 11. XRD patterns of alloy 2 as prepared as well as annealed at the different temperatures.

cooling did not occur. However, the austenitic phase transformation (HCP to FCC) temperature is a function of heating rate [47]. At this point, it is assumed that the allotropic transformation is connected with grain growth. The FCC phase is retained upon cooling to ambient temperature and with increasing temperature the content of HCP phase is reduced. Further investigations of structural transformation in electrodeposited nanocrystalline alloy sample with high content of Co are performed actually.

As in the case of alloy 1, based on the DSC curve (Figure 10), the analysis of structural transformations of Ni–Co deposits (alloy 2) induced by heating were carried out using samples annealed at temperatures of 280, 350 and 550 °C.

SEM micrographs of annealed alloy 2 are shown in Figure 12. The platelet structure is preserved; however, the top of the particles consists of the platelets with reduced size. Additionally, single particle grains are much better formed in comparison to the as-prepared sample (Figure 12).

Magnetic properties of nanocrystalline deposits

Electrodeposited nanostructured ferromagnetic materials such as Ni and Ni–Fe alloys exhibit desirable soft magnetic properties such as low coercivity, increased electrical resistivity and grain size independent saturation magnetization [47]. Magnetic saturation of electrodeposited ferromagnetic materials is only dependent on the composition [49]. The potential application of cobalt based nanocrystalline alloys has attracted attention because of their higher saturation magnetization compared with Ni and permalloy (Ni–20 wt% Fe) type electrodeposits.

The samples obtained after pressing were heated up to 600 °C in an argon atmosphere in order to achieve the thermal stabilization of alloy structure. Upon application of a weak magnetic field, the magnetization increases rapidly to a high value called the saturation magnetization (Figure 13), which is in general a function of temperature. The relative magnetic permeability increases in the temperature range from 180 to 250 °C for alloy 1 and to 430 °C for alloy 2 with a peak value at

Table 5. Phase composition and size of crystallites of electrodeposited and annealed alloy 2

Alloy	Crystal structure	Grain size, nm	*a* / Å	*c* / Å	Cell volume, Å^3
Alloy 2 (as prepared)	HCP	20	2.506	4.069	22.126
Alloy 2 (annealed at 280°C)	HCP	21	2.507	4.071	22.159
Alloy 2 (annealed at 350 °C)	HCP	19	2.508	4.071	22.177
Alloy 2 (annealed at 550 °C)	FCC	50	3.547	–	44.616
	HCP	7	2.479	4.257	22.660

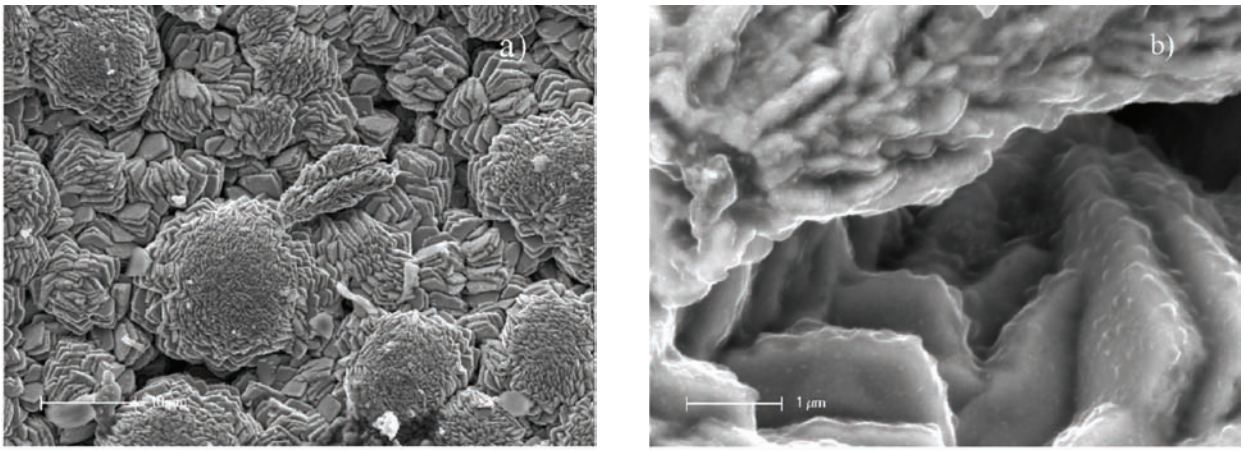

Figure 12. SEM micrographs of Ni–Co deposits on copper substrate prepared out of an electrolyte with concentration ratio Ni^{2+}/Co^{2+} = = 0.25, j = 65mAcm^{-2} (alloy 2), upon annealing at 550 °C; a) magnification 2000×, b) magnification 20000× (SE, accelerating voltage 10 kV).

250 (alloy 1) and 430 °C (alloy 2). A decrease in the free volume, a decrease in the content minimal value of the chaotically distributed dislocations and a reduction in the content of microstrains took place in this temperature interval.

The increase in magnetic permeability is a consequence of the described structural changes during heating. All of these features ensure greater mobility of the magnetic domain walls and their better directionality, consequently increasing the magnetic permeability. In the temperature range 250 to 370 °C the relative magnetic permeability of alloy 1 decreases rapidly, reaching Curie temperature at approximately 370 °C, close to the value of pure Ni (627 K) [39]. The slightly higher value of the Curie temperature can be attributed to the content of Co in the sample (see Table 2) The relative magnetic permeability for alloy 2 decreases in the temperature range of 420 to 525 °C. The Curie temperature of this sample is related to the relative high content of Ni, reducing the Curie temperature from the value of pure Co of 1388 K [48] to the actual one.

CONCLUSION

The structures as well as morphology of the disperse Ni–Co alloy galvanostatically deposited from ammonium nickel and cobalt sulfate solutions on Cu cathodes depend on the deposition current density as well as the bath composition. FCC phase is the predominant phase in the alloy deposits at the Ni-rich side. A decrease in the Ni concentration in the alloy deposits causes the increase in the concentration of HCP phase in the crystalline part of the deposit. A decrease in the deposition current density results in an increased amount

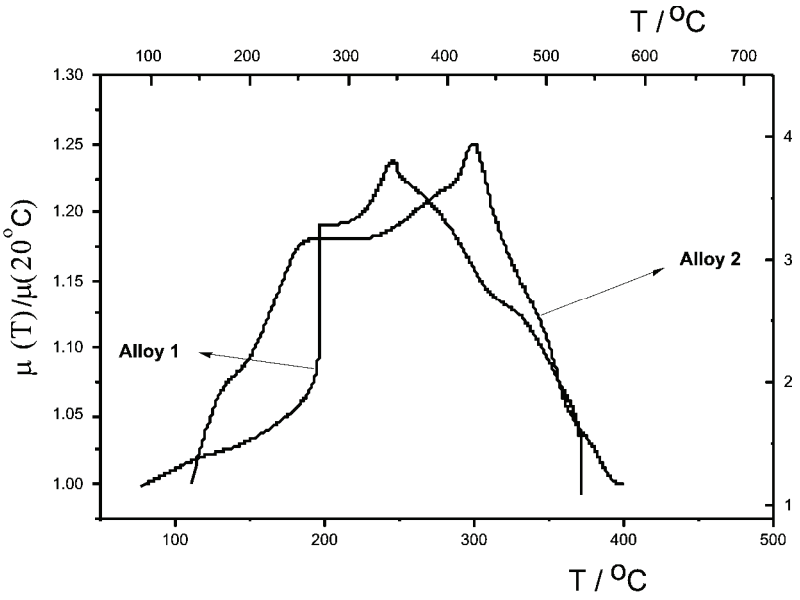

Figure 13. Temperature dependence of relative magnetic permeability of alloys.

of the HCP phase in the deposit and the crystal grain growth of FCC and HCP phases. HCP phase is the dominant phase in deposits with a higher content of cobalt. Increase of the deposition current density in electrolytes with a concentration ratio Ni^{2+}/Co^{2+} = 1 leads to a decrease of HCP phase content in the deposits, the crystal grains growth of the FCC phase and the transformation of the HCP phase into the FCC phase. A significant thermal effect upon heating of nanocrystalline Ni–Co alloy deposits has been observed. In Co--rich samples, structural changes during heating were attributed to the phase transformation of HCP to FCC. The relative magnetic permeability strongly depends on the Ni^{2+}/Co^{2+} ratio in the alloys, showing the strong influence of a material with low Curie temperature (Ni) on a material with a high Curie temperature (Co).

Acknowledgments

The investigation was partially supported by the Ministry of Science and Technlogical Development of the Republic of Serbia, under the project No. 142025. The support by the I.K. "Experimental Materials Science – Nanostructured Materials", a college for PhD students at the University of Vienna, is greatly appreciated by L.R.

REFERENCES

[1] H. Gleiter, Nanocrystalline materials, Prog. Mater. Sci.**33** (1989) 223–315.

[2] R.P. Andres, R.S. Averback, W.L. Brown, L.E. Brus, W.A. Goddard III, S.G. Kaldor, J. Mater. Res. **4** (1989) 704–736.

[3] M.A. Meyers, A. Mishra, D.J. Benson, Prog. Mater. Sci. **51** (2004) 427–556.

[4] U. Erb, Nanost. Mater. **6** (1995) 533–538.

[5] N. V. Myung, K. Nobe, J. Electrochem. Soc. **148** (2001) 136–144.

[6] D.Y. Park, K.S. Park, J.M. Ko, D.H. Cho, S.H. Lim, W.Y. Kim, B.Y. Yoo, N.V. Myung, J. Electrochem. Soc.153 (2006) 814–821.

[7] A. Bianco, G. Gusmano, R. Montanari, G. Montesperelli, E. Traversa, Thermochimica Acta **269/270** (1995) 117––132.

[8] A. Calusaru, Electrodeposition of Powders from Solutions, Elsevier, New York, 1979.

[9] C.A.C. Souza, J.E. May, A.T. Machado, A.L.R. Tachard, E.D. Bidoia, Surf. Coat. Technol **190** (2005) 75–82.

[10] K.I. Popov, M.G. Pavlović, Electrodeposition of metal powders with controlled particle grain size and morphology", in: Modern Aspects of Electrochemistry, Vol. 24, R.E. White, B.E. Conway, J.O'M. Bockris (Eds.), Plenum Press, New York, 1993, Ch. 6.

[11] A. Maričić, M. Spasojević, L. Rafailović, V. Milovanović, L. Ribić-Zelenović, Mat. Sci. Forum **453/454** (2004) 411–416.

[12] L. Ribić-Zelenović, L. Rafailović, M. Spasojević, A. Maričić, Sci. Sintering 38 (2006) 145–153.

[13] L. Ribić-Zelenović, L. Rafailović, M. Spasojević, A. Maričić, Physica B, **403** (2008) 2148–2154.

[14] A.Vicenzo, P.L.Cavallotti, Electrochim. Acta **49** (2004) 4079–4089.

[15] S.Armyanov, S.Vitkova, Surf. Technol. **7** (1978) 319––329.

[16] J. Scoyer, R. Winand. Surf. Technol. **5** (1977) 169–204.

[17] T Cohen-Hyams, W.D. Kaplan, J. Yahalom, Electrochem. Solid State Lett. **5** (2002) 75.

[18] H. Li, F. Ebrahimi, Mater. Sci. Eng. **A** 347 (2003) 93.

[19] S.H.Kim, K.T. Aust, U. Erb, F.Gonzales, G. Palumbo, Scripta Mater. **48** (2003) 1379–1384.

[20] E. Gómez, S. Pané, E. Vallés, Electrochim. Acta **51** (2005) 146–153.

[21] E. Gómez, S. Pané, X. Alcobe, E. Vallés, Electrochim. Acta **51** (2006) 5703–5709.

[22] D. Kim, D.Y .Park, B.Y.Yoo, P.T.A.Sumodjo, N.V. Myung, Electrochim. Acta **48** (2003) 819–830.

[23] N.V. Myung, D.-Y .Park, B.-Y.Yoo, P.T.A .Sumodjo, J. Magn. Mag. Mater. **265** (2003) 189–198.

[24] I.Z. Rahman, M.V. Khaddem-Mousavi, A.A.Gandhi, T.F.Lynch, M.A.Rahman, J. Phys.: Conference Series **61** (2007) 523–528.

[25] D.Minić, L.D. Rafailović, J. Wosik, G.E. Nauer, in: Handbook of Materials Science Research, Nova Sciense Publishers Inc., 2009, Ch. 10.

[26] V.D. Jović, V. Maksimović, M.G. Pavlović, V. Maksimović, J. Solid State Electrochem. **10** (2006) 959–966.

[27] V.D. Jović, B.M. Jović, M.G. Pavlović, Electrochim. Acta **51** (2006) 5468–5477.

[28] L.D. Rafailović, H.P. Karnthaler, T. Trišović, D.M. Minić, Mater. Chem. Phys. (submitted).

[29] L.D. Rafailović, W. Artner, G.E. Nauer, D.M. Minić, Thermochim. Acta (2009), doi: 10.1016-j.tca.2009.07.007.

[30] L.D. Rafailović, A.M. Maričić, W. Artner, G.E. Nauer, D.M. Minić, Sci. Sinter. **41** (2009) 135–142.

[31] M. Spasojević, A. Maričić, L. Rafailović, Sci. Sinter. **36** (2004) 105–112.

[32] S. Ranđić, A. Maričić, L. Rafailović, M. Spasojević, M.M. Ristić, Sci. Sinter. **38** (2006) 139–144.

[33] L. Ribić-Zelenović, L. Rafailović, M. Spasojević, A. Maričić, J. Optoelectron. Adv. Mater. **9** (2007) 2681–2685.

[34] R. Simeunović, M. Spasojević, L. Rafailović, A. Maričić, Proceedings of the Congress of Physicians of Serbia and Montenegro, Petrovac, Serbia and Montenego, 2004, pp.149–152.

[35] M. Spasojević, A. Maričić, L. Rafailović, B. Jordović, 5th Yugoslav Materials Research Society Conference YUCOMAT 2003, Book of Abstracts, Herceg Novi, 2003, p. 64.

[36] L.Rafailović, A.Maričić, M.Spasojević, L.Ribić-Zelenović, R.Simeunović, XVIII Congress of Chemists and Technologists of Macedonia, Book of Abstracts, Ohrid, Macedonia, 2004, p 421.

[37] L.D. Rafailović, P. F. Rogl, D.M. Minić, H. P. Karnthaler, First Joint Metting of Dreiländertagung and Multinational Congress on Microscopy, Vol. 3, Material Science, MC 2009, Graz, Austria, 2009, p. 125.

[38] G.M. Chow, Y.Y. Li, Y.K. Hwu, Mater. Phys. Mech. **1** (2000) 67–72.
[39] D.M. Minić, The Applied Electrochemistry, Faculty for Physical Chemistry, Belgrade, 1996.
[40] K.I. Popov, S.S. Djokić, B.N. Grgur, Fundamental Aspects of Electrometallurgy, Kluwer Academic Press, New York, 2002.
[41] H. Rietveld, J. Appl. Crystallogr. **2** (1969) 65–71.
[42] T.B. Massalski, Binary Alloy Phase Diagrams, ASM International, Materials Park, OH,1991. T.B. Massalski, Binary Alloy Phase Diagrams, ASM International, Materials Park, OH, 1991.
[43] F. Czerwinski, A. Zielinska-Lipiec, J.A. Szpunar, Acta Mater. **47** (1999) 2553–2566.
[44] B. Bozzini, G. Giovannelli and P.L. Cavallotti, J. Appl. Electrochem. **30** (2000) 591–594.
[45] L. Peraldo Bicelli, B. Bozzini, C. Mele, L. D'Urzo, Int. J. Electrochem. Sci. **3** (2008) 356–408.
[46] L.C. Chen, F. Spaepen, J. Appl. Phys. **69** (1991) 679––688.
[47] N. Wang, Z. Wang, K.T. Aust, U. Erb, Acta Mater. **45** (1997) 1655–1669.
[48] G. Hibbard, K. T. Aust, G. Palumbo, U.Erb, Scripta Mater. **44** (2001) 513–518.
[49] N.V. Myung, D.-Y .Park, B.-Y.Yoo, P.T.A .Sumodjo, J. Magnet. Mag. Mater. **265** (2003) 189–198.
[50] G. Hibbard, K. T. Aust, G. Palumbo, U.Erb, Scripta Mater. **44** (2001) 513–518.
[51] C. Kittel, Introduction to Solid State Physics, 8th ed., Willey, 2005.

IZVOD

DEPOZICIJA I KARAKTERIZACIJA NANOSTRUKTURNIH PRAHOVA NIKAL–KOBALT LEGURE

Lidija D. Rafailović[1], Dragica M. Minić[2]

[1]Physics of Nanostructured Materials, Faculty of Physics,University of Vienna, Austria
[2]Fakultet za fizičku hemiju, Univerzitet u Beogradu, Srbija

(Pregledni rad)

Nanostrukturne nikal–kobalt legure su dobijene galvanostatski na Cu supstratima iz amonijum sulfat-hloridnih elektrolita. Proučavani su uticaj gustine struje depozicije i sastav elektrolita (odnos Ni^{2+}/Co^{2+}) na fazni sastav i morfologiju depozita. Pokazano je da sastav kupatila i gustina struje značajno utiču na mehanizam rasta odnosno na sastav i mikrostrukturu depozita kao i na veličinu zrna i morfologiju površine. Kada se elektrodepozicija izvodi na visokim nadnaponima, daleko od ravnotežnih uslova, grade se smeše Ni i Co površinski centrirane kubne strukture (FCC) dok se pri nižim nadnaponima , kao i pri višim sadržajima kobalta u elektrolitu grade Co depoziti heksagonalne gusto pakovane strukture (HCP) praćeni malom brzinom izdvajanja vodonika. Porast količine HCP faze u nanokristalnim depozitima je posledica kako porasta sadržaja kobalta u depozitu tako i smanjenja gustine struje depozicije. Takođe su proučavani efekti strukturnih promena na magnentna svojstva nanokristalnih prahova elektrohemijski dobijenih u temperaturskom intervalu od sobne temperature do 600 °C. Pokazano je da svaki stupanj strukturnih promena izaziva odgovarajuće promene u magnetnoj permeabilnosti dobijenih legura.

Ključne reči: Nanostrukturni materijali • Elektrohemijska depozicija • Morfologija • Toplotni tretman
Key words: Nanostructured materials • Electrochemical deposition • Morphology • Thermal treatment